NANO LETTERS

2008
Vol. 8, No. 8
2224-2228

Single-Walled Carbon Nanotube Thin Film Emitter−Detector Integrated Optoelectronic Device

Mikhail E. Itkis, Aiping Yu, and Robert C. Haddon*

Center for Nanoscale Science and Engineering, Departments of Chemistry and Chemical and Environmental Engineering, University of California, Riverside, California 92521-0403

Received March 20, 2008

ABSTRACT

We use the suspended single-walled carbon nanotube (SWNT) thin film technology to assemble the first prototype of an integrated optoelectronic SWNT device, a SWNT optocoupler in which a SWNT emitter and a SWNT detector couple two electrical circuits by the transmission of a signal through the optical channel. Our experiments show that the integrated SWNT emitter/SWNT detector is an ideal couple in which the broadband wavelength character of the emission matches the broadband detection capabilities.

In recent years, single-walled carbon nanotube (SWNT) optoelectronics has emerged as one of the most interesting areas of carbon nanotube science and applications.[1–10] The ability to detect incident light was demonstrated for individual SWNTs,[1,4] SWNT bundles,[7,11] and SWNT films,[12–14] although the photoresponse was found to be weak because of the formation of strongly bound excitons.[4,15,16] A significant improvement of the photoresponse was achieved by dissociation of the excitons in the large internal electric field that could be realized in a field-effect transistor (FET) configuration.[9] Recently, we demonstrated that the photoresponse can be dramatically enhanced by suspending SWNT films in vacuum between electrical contacts to take advantage of the strong bolometric effect.[6]

Another promising class of optoelectronic applications relates to the ability of carbon nanotubes to emit light on the passage of an electric current in the form of a discrete spectrum resulting from electroluminescence due to interband transitions,[3,5] or as continuum blackbody radiation spectra originated from Joule heating,[17–19] or due to a combination of both components.[20] The integration of individual SWNT devices into functioning electronic or optoelectronic logic circuits is an important step in the further development of SWNT−based electronics. In the present manuscript, we use the suspended SWNT thin film technology to demonstrate the first prototype of an integrated optoelectronic SWNT device, a SWNT optocoupler in which a SWNT emitter and a SWNT detector couple two electrical circuits by the transmission of a signal through the optical channel.

A schematic of the SWNT optocoupler is shown in Figure 1a; the optical microscope image of the device prototype is presented in Figure 1b. For device preparation, we utilized free-standing SWNT films of electric arc produced and purified SWNTs prepared by vacuum filtration according to the procedure described in the literature.[6,21,22] The detector was made by suspending a narrow ribbon of SWNT film across the opening of a sapphire ring; a second sapphire ring was used to support a SWNT thin film emitter in a similar way. The two sapphire rings were attached by thermally conducting adhesive paste back to back so the SWNT emitter and detector were facing each other at a separation of 2.0 mm. The dimensions (length × width × thickness) of the SWNT detector and emitter were 1 mm × 0.24 mm × 100 nm and 2.2 mm × 0.64 mm × 150 nm, respectively. The sapphire rings were mechanically and thermally attached to the coldfinger of a continuous flow optical cryostat with the sample space maintained in vacuum.

Figure 1c shows the temperature dependence of the resistance of the SWNT detector and emitter films, both of which show semiconducting behavior with a strong increase in the resistance with decreasing temperature. It is known that the resistance of SWNT network and its temperature dependence are dominated by the role of intertube junctions,[23–26] with Schottky barriers defining the semiconducting behavior despite of the presence of metallic SWNTs.[27] This strong temperature dependence is especially important in achieving a highly sensitive IR detector; in the present work, the SWNT detector film was chosen to be thinner than the emitter film in order to provide a stronger temperature dependence of resistance: $R(30\ \mathrm{K})/R(300\ \mathrm{K}) \approx 4$ (detector), 1.5 (emitter).

* Corresponding author. E-mail: haddon@ucr.edu.

10.1021/nl080814u CCC: $40.75
Published on Web 07/04/2008

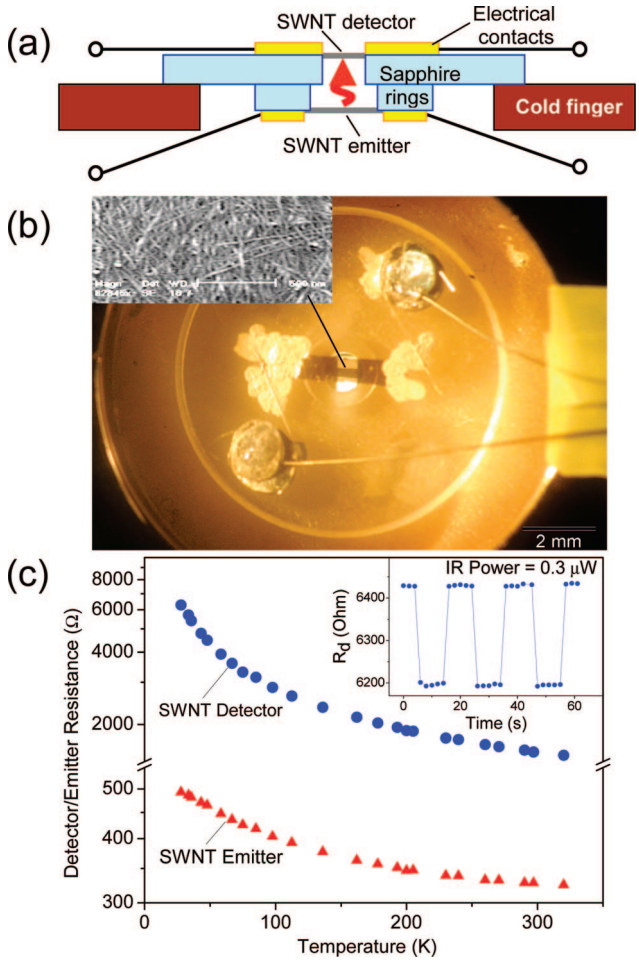

Figure 1. (a) Schematic of the SWNT optocoupler: SWNT thin film emitter and detector are mounted face-to-face on two sapphire rings so the radiation from SWNT emitter can be sensed by the detector. (b) Optical microscope image of the SWNT optocoupler. Both SWNT emitter and detector films are ultrathin and semitransparent, so the narrow strip of SWNT detector (on the back) can be seen through the SWNT emitter film (in front). Inset: SEM image of the SWNT film. (c) Semiconducting temperature dependence of resistance $R(T)$ of SWNT film emitter (red triangles) and SWNT film detector (blue circles). Inset: SWNT film detector response to square-wave pulses of 0.3 μW radiation of IR LED.

At first, the sensitivity of the SWNT detector was tested by utilizing an external IR LED (peak emission wavelength 940 nm) situated outside the cryostat with incident IR power at the detector of 0.3 μW. In this configuration, using lock-in amplifier, we registered a response of 470 μV corresponding to a responsivity >1500 V/W and signal-to-noise ratio >1000 at an operating temperature of 28 K, which is similar to our previously reported results.[6] As we demonstrated, this strong photoresponse is associated with the efficient transfer of the power of the IR radiation to heat in the SWNT lattice as a result of strong electron−phonon coupling in the 1D-SWNT system; this serves to raise the temperature of the SWNT film, and the photoresponse is observed via the strong temperature dependence of the resistance of the ultrathin SWNT films.

In order to realize a functioning SWNT optocoupler device, square-wave voltage pulses (Figure 2a) were applied to the SWNT emitter circuit which includes a 1 kΩ load resistor connected in series with the SWNT film, and we observed a strong response in the SWNT detector (Figure 2b), similar in amplitude to its response to the radiation from an external IR LED. From the temporal variation of the voltage across the SWNT emitter film during the pulse (Figure 2c), we found that its resistance (R_{EM}) decreases from 455 Ω to 370 Ω (Figure 2d) which according to $R_{EM}(T)$ (Figure 1c) corresponds to an average temperature of the SWNT film of 105 K, compared with the base temperature of 28 K (Figure 2e). Increasing the amplitude of the driving square-wave pulses from V_{GEN} = 1.16 V (voltage drop on SWNT emitter film, V_{EM} = 310 mV) to 3.8 V (V_{EM} = 950 mV) causes a stronger decrease of the emitter resistance from 455 to 330 Ω (Figure 2d) corresponding to an average temperature increase from 28 to 180 K (Figure 2e), which is accompanied by a factor of 10 increase in the detector response.

The radiation from the IR emitter under voltage pulses V_{GEN} = 1.16 V modulates the SWNT detector resistance between ~6.5 kΩ and ~4.1 kΩ which corresponds to temperature modulation between the base temperature 28 K and the average temperature 55 K (Figure 2f) according to $R_{DET}(T)$ (Figure 1c). In addition to the emitter radiation, a second pathway for power transmittance from the SWNT emitter to the SWNT detector is available through the thermal conductance of the supporting sapphire rings (Figure 1). In order to evaluate the contribution of this heat conduction channel, we placed a GaAlAs thermometer next to the SWNT detector on the supporting sapphire ring in addition to the thermometer attached to the coldfinger of the cryostat. We found that the temperature modulation of the supporting substrate of the SWNT detector does not exceed 0.05 K (Figure 2g), ~500 times smaller than the modulation of SWNT detector temperature thus confirming the dominant role of the emitter radiation in the power transmittance.

To a first approximation, the Joule heat generated by the passage of a current through the suspended SWNT film generates a parabolic temperature profile $T(x)$ as a distributed power source in a one-dimensional (1D) heat flow geometry.[20,28] In such a case, the maximum temperature increase in the center of the emitter is 1.5 times higher than the average temperature increase. Because of the T^4 dependence of the power of the blackbody radiation, it is predominantly emitted from the central region of the suspended SWNT film where the temperature is close to the maximum.[20,28] Figure 3a presents blackbody radiation spectra calculated using Planck's law for spectral radiance $I(\lambda,T) = (2hc^2/\lambda^5)/(e^{hc/\lambda kT} - 1)$ for two maximum temperatures (144 and 256 K), which correspond to average temperatures of 105 and 180 K, respectively (Figure 3de); the resulted spectral emission maxima are located at wavelengths of $\lambda \approx 11.3$ and 20 μm, respectively. The intensity of the spectral curve corresponding to 256 K is about an order of magnitude stronger than for 144 K matching the difference of the amplitude of the SWNT detector response and supporting the conclusion that the blackbody radiation is the primary source of the emitter−detector communication.

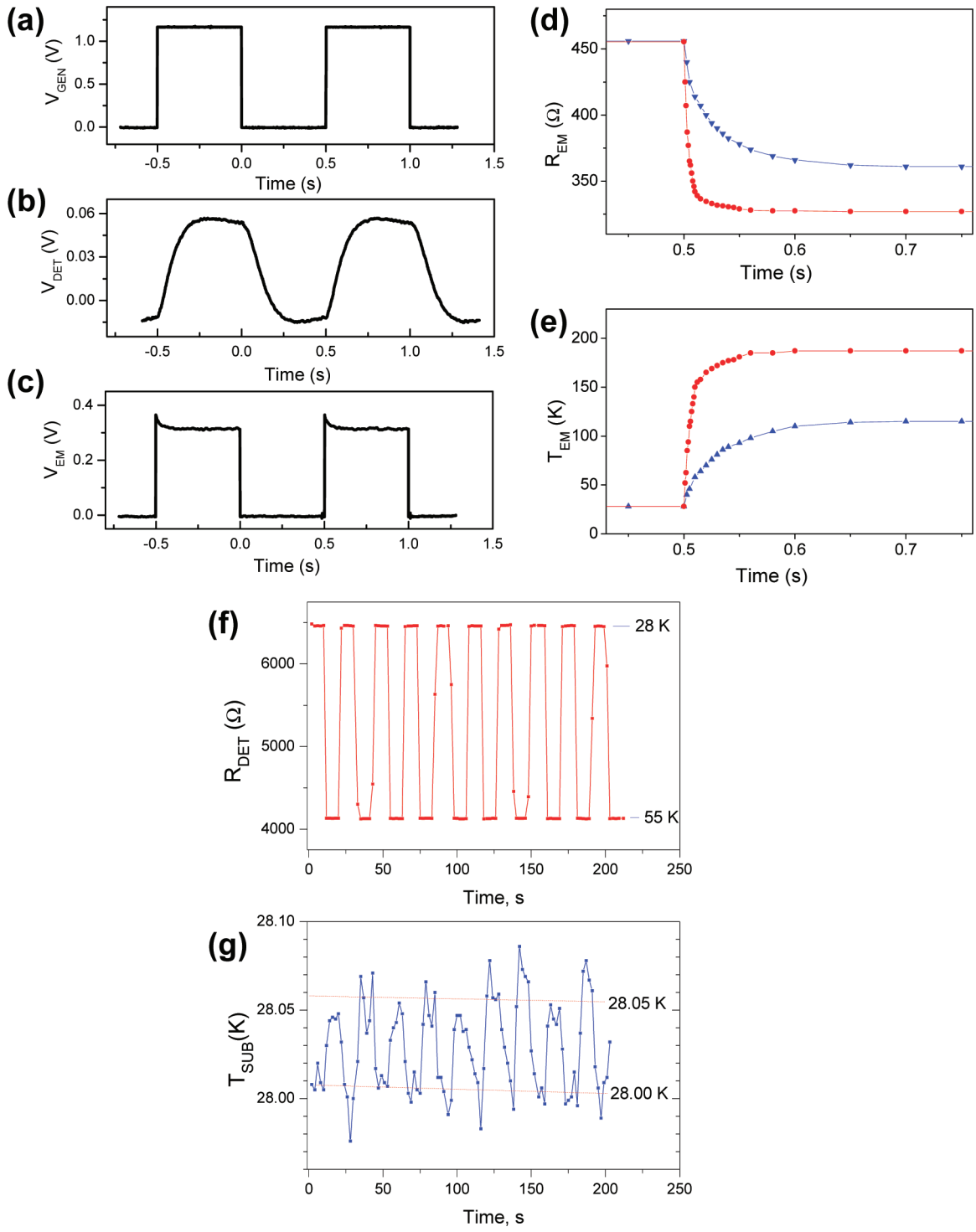

Figure 2. Operation of SWNT optocoupler: (a) Square-wave voltage pulses from a function generator V_{GEN} are used to drive the SWNT emitter circuit. (b) Oscillogram of SWNT detector response V_{DET} to the radiation of SWNT emitter under the driving pulses. (c) Oscillogram of the voltage drop on the SWNT emitter, $V_{EM} = V_{GEN} - V_{LOAD}$, where V_{LOAD} is a voltage drop across 1 kΩ load resistance. (d) Change of the emitter resistance R_{EM} during square-wave driving pulses of amplitude 1.16 V (blue triangles) and 3.8 V (red circles). (e) Average temperature of SWNT emitter T_{EM} under driving pulse of amplitude 1.16 V (blue triangles) and 3.8 V (red circles). (f) Response of the SWNT detector resistance R_{DET} (red) to the driving pulses through the emitter circuit. (g) Temperature of supporting sapphire substrate T_{SUB} (blue) in response to the driving pulses as in (f).

Figure 3b shows the spectral absorbance of a 100 nm thick SWNT film in the range 3−50 μm. The absorbance is broadband and extends from the UV to the FIR[29] and even to the Terahertz[7,11] and Megahertz[30] regions. The SWNT film is a far more efficient absorber of IR radiation than the narrow band or extrinsic semiconductors currently utilized for photodetection in this spectral range.[6] It is worth noting that the increase of the absorbance toward longer wavelengths (Figure 3b) partially compensates for the decrease in intensity of the blackbody radiation at lower maximum

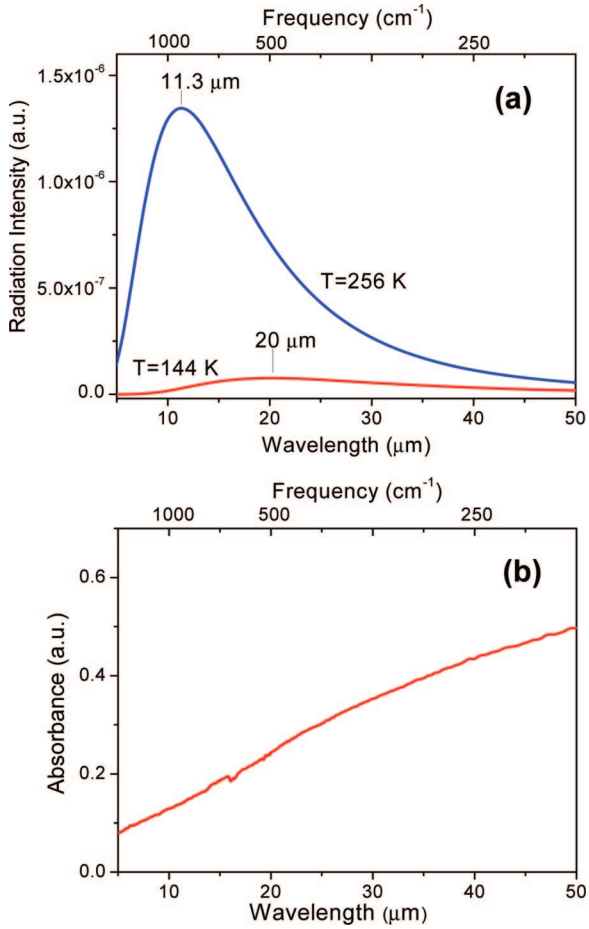

Figure 3. Spectral characteristics of SWNT emitter and detector: (a) Spectra of blackbody radiation of SWNT film at temperatures of 256 and 144 K calculated using Planck's law. (b) Spectral dependence of the absorbance of a 100 nm thick SWNT film used in the bolometric detector.

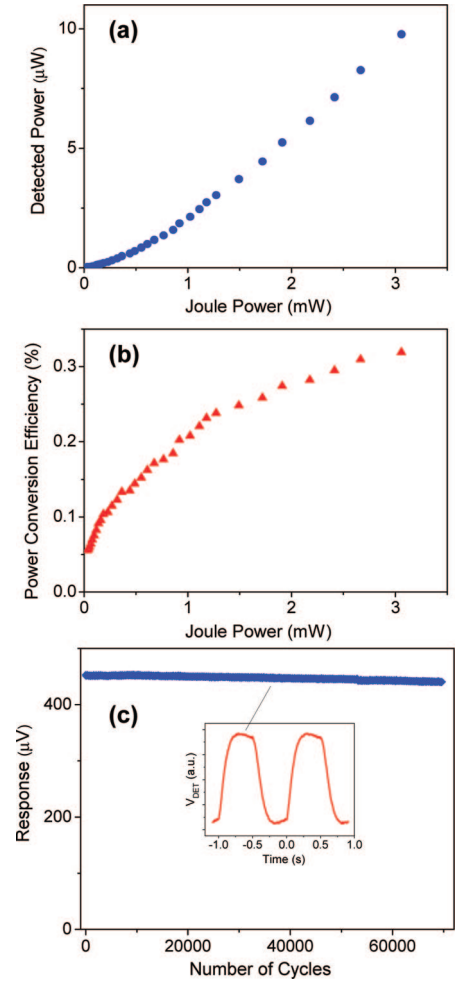

Figure 4. (a) Power detected by the SWNT bolometer as a function of Joule power driving the SWNT emitter. (b) Power conversion efficiency of the SWNT optocoupler increases with increasing Joule power because the blackbody radiation channel of the power transfer dominates the solid state thermal conductivity channel with increasing temperature modulation. (c) Long-term stability of SWNT optocoupler under 1.16 V square-wave driving pulses (emitter temperature modulation between 28 and 105 K) over 70 000 cycles. Inset shows oscillogram of the SWNT detector response during this test.

temperature of the emitter. Thus, the SWNT emitter/SWNT detector is an ideal couple in which the broadband wavelength character of the emission matches the broadband detection capabilities.

It has been shown that the application of high amplitude excitation pulses to a suspended individual quasi-metallic SWNT can lead to a rise in temperature of 1200 K which shifts the emission spectra toward the visible spectral range with involvement of interband transitions.[20] The SWNT thin film optocoupler does not require such high excitation power and the temperature modulations can be held at the 10−100 K level thus prolonging the device lifetime. For example, emission of the SWNT film heated to 144 K (Figure 3a, low intensity spectrum) provides signal-to-noise ratio >1000 in transmitting the signal within the SWNT emitter−detector optocoupler.

Figure 4a shows that IR power registered by the SWNT detector P_{DET} increases superlinearly as a function of the Joule power P_{JL} supplied to the SWNT emitter; such an increase of the efficiency P_{DET}/P_{JL} can be understood by considering the fact that, in vacuum, the Joule heat which is generated is dissipated mainly through two channels of heat transport: the thermal conductivity (κ) along the SWNT film to the substrate through the electrical contact $Q_{TC} \sim \kappa(T)*\Delta T$ and the blackbody radiation $Q_{BB} \sim \sigma_{S-B}T^4$ (σ_{S-B} is Stephan−Boltzmann constant) with the contribution of the last term increasing strongly with the temperature of the SWNT emitter film. Taking into account the emitter−detector geometry with a SWNT film separation of 2 mm, we estimate that only 3% of emitted radiation reaches the detector. The efficiency of the power transmittance can be readily improved by a factor of 10 simply by closing the distance between the emitter and the detector which could be accomplished by using a perforated thin film of mylar with the SWNT emitter and detector on opposite sides. This would allow a significant reduction in the driving power and the amplitude of the modulation of the SWNT emitter temperature thus extending the long-term stability and lifetime of the SWNT-based optocoupler. Even in its current state, the assembled SWNT emitter−detector optocoupler shows high long-term reliability. In Figure 4c, we show the performance of the device over 70 000 cycles at a frequency 1 Hz; under square-

wave pulses $V_{GEN} = 1.16$ V (Figure 3a), we observed very little decrease of the detector response and the signal of the detector which was initially 450 μV, decreased by less than 2% to 442 μV at the completion of the test.

Applications based on SWNT thin film technology are now recognized as a near term alternative[8,31–33] to the development of nanoelectronics based on individual SWNTs.[10] Successful applications of SWNT thin films have been demonstrated in the areas of gas sensors and biosensors,[34,35] field effect transistors, transparent conducting electrodes for large area organic flexible optoelectronics,[8,22,33] thin film coatings for electromagnetic shielding,[30] and in fuel cells.[36] Further development of the SWNT thin film optocoupler will incorporate thin film photolithography which would allow the manufacture of multichannel arrays of SWNT-based optocouplers with pixel size of 30−20 μm, which is comparable to current focal plane array technology. Such size decrease would permit a significant reduction of the power per individual optocoupler and a significantly faster response time which is an important characteristic of the optocoupler performance. In this report, we have already reduced the detector size by a factor of 3 in comparison with our first publication[6] without decreasing the responsivity of the detector. The performance of the SWNT optocoupler can be optimized for room temperature applications by using chemically functionalized[25] or pure semiconducting SWNTs with high temperature coefficient of resistance.

Acknowledgment. This research was supported by DOD/DMEA under Award Nos. H94003-06-2-0608 and H94003-07-2-0703.

References

(1) Freitag, M.; Martin, Y.; Misewich, J. A.; Martel, R.; Avouris, P. *Nano Lett.* **2003**, *3* (8), 1067–1071.
(2) Misewich, J. A.; Martel, R.; Avouris, P.; Tsang, J. C.; Heinze, S.; Tersoff, J. *Science* **2003**, *300*, 783–786.
(3) Freitag, M.; Chen, J.; Tersoff, J.; Tsang, J. C.; Qiang, F.; Liu, J.; Avouris, P. *Phys. Rev. Lett.* **2004**, *93* (7), 076803.
(4) Qiu, X.; Freitag, M.; Perebeinos, V.; Avouris, P. *Nano Lett.* **2005**, *5*, 749–752.
(5) Chen, J.; Perebeinos, V.; Freitag, M.; Tsang, J.; Fu, Q.; Liu, J.; Avouris, P. *Science* **2005**, *310*, 1171–1174.
(6) Itkis, M. E.; Borondics, F.; Yu, A.; Haddon, R. C. *Science* **2006**, *312*, 413–416.
(7) Tarasov, M.; Svensson, J.; Weis, J.; Kuzmin, L.; Campbell, E. *JETP Lett.* **2006**, *84* (5), 267–270.
(8) Gruner, G. *J. Mater. Chem.* **2006**, *16*, 3533–3539.
(9) Lee, J. U.; Codella, P. J.; Pietrzykowski, M. *Appl. Phys. Lett.* **2007**, *90*, 053103.
(10) Avouris, P.; Chen, Z.; Perebeinos, V. *Nat. Nanotechnol.* **2007**, *2*, 605–615.
(11) Fu, K.; Zannoni, R.; Chan, C.; Adams, S. H. J. N.; Polizzi, E.; Yngvesson, K. S. *Appl. Phys. Lett.* **2008**, *92*, 033105.
(12) Levitsky, I. A.; Euler, W. B. *Appl. Phys. Lett.* **2003**, *83* (9), 1857–1859.
(13) Fujiwara, A.; Matsuoka, Y.; Matsuoka, Y.; Suematsu, H.; Ogawa, N.; Miyano, K.; Kataura, H.; Maniwa, Y.; Suzuki, S.; Achiba, Y. *Carbon* **2004**, *42*, 919–922.
(14) Mohite, A.; Chakraborty, S.; Gopinath, P.; Sumanasekera, G. U.; Alphenaar, B. W. *Appl. Phys. Lett.* **2005**, *86*, 061114.
(15) Perebeinos, V.; Tersoff, J.; Avouris, P. *Phys. Rev. Lett.* **2004**, *92* (25), 257402.
(16) Wang, F.; Dukovic, G.; Brus, L. E.; Heinz, T. *Science* **2005**, *308*, 838–841.
(17) Sveningsson, M.; Jonsson, M.; Nerushev, O. A.; Rohmund, F.; Campbell, E. E. B. *Appl. Phys. Lett.* **2002**, *81* (6), 1095–1097.
(18) Li, P.; Jiang, K.; Liu, M.; Li, Q.; Fan, S.; Sun, J. *Appl. Phys. Lett.* **2003**, *82* (11), 1763–1765.
(19) Wei, J.; Zhu, H.; Wu, D. *Appl. Phys. Lett.* **2004**, *84* (24), 4869–4871.
(20) Mann, D.; Kato, Y. K.; Kinkhabwala, A.; Pop, E.; Cao, J.; Wang, X. R.; Zhang, L.; Wang, Q.; Guo, J.; Dai, H. J. *Nat. Nanotechnol.* **2007**, *2*, 33–38.
(21) Hennrich, F.; Lebedkin, S.; Malik, S.; Tracy, J.; Barczewski, M.; Rosner, H.; Kappes, M. *Phys. Chem. Chem. Phys.* **2002**, *4*, 2273–2277.
(22) Wu, Z.; Chen, Z.; Du, X.; Logan, J. M.; Sippel, J.; Nikolou, M.; Kamaras, K.; Reynolds, J. R.; Tanner, D. B.; Hebard, A. F.; Rinzler, A. G. *Science* **2004**, *305*, 1273–1276.
(23) Kaiser, A. B.; Dusberg, G.; Roth, S. *Phys. Rev. B* **1998**, *57*, 1418–1421.
(24) Hu, L.; Hecht, D. S.; Gruner, G. *Nano Lett.* **2004**, *4*, 2513–2517.
(25) Bekyarova, E.; Itkis, M. E.; Cabrera, N.; Zhao, B.; Yu, A.; Gao, J.; Haddon, R. C. *J. Am. Chem. Soc.* **2005**, *127*, 5990–5995.
(26) Itkis, M. E.; Borondics, F.; Yu, A.; Haddon, R. C. *Nano Lett.* **2007**, *7* (4), 900–904.
(27) Fuhrer, M. S.; Nygard, J.; Shih, L.; Forero, M.; Yoon, Y.-G.; Mazzoni, M. S. C.; Choi, H. J.; Ihm, J.; Louie, S. G.; Zettl, A.; McEuen, P. L. *Science* **2000**, *288*, 494–497.
(28) Pop, E.; Mann, D.; Cao, J.; Wang, Q.; Goodson, K.; Dai, H. *Phys. Rev. Lett.* **2005**, *95*, 155505.
(29) Itkis, M. E.; Niyogi, S.; Meng, M.; Hamon, M.; Hu, H.; Haddon, R. C. *Nano Lett.* **2002**, *2*, 155–159.
(30) Xu, H.; Anlage, S. M.; Hu, L. B.; Gruner, G. *Appl. Phys. Lett.* **2007**, *90* (18), 183119.
(31) Kaempgen, M.; Duesberg, G. S.; Roth, S. *Appl. Surf. Sci.* **2005**, *252*, 425–429.
(32) Zhang, M.; Fang, S.; Zakhidov, A. A.; Lee, S. B.; Aliev, A. E.; Williams, C.; Atkinson, K. R.; Baughman, R. H. *Science* **2005**, *309*, 1215–1219.
(33) Zhang, D.; Ryu, K.; Liu, X.; Polikarpov, E.; Ly, J.; Tompson, M. E.; Zhou, C. *Nano Lett.* **2006**, *6* (9), 1880–1886.
(34) Bekyarova, E.; Davis, M.; Burch, T.; Itkis, M. E.; Zhao, B.; Sunshine, S.; Haddon, R. C. *J. Phys. Chem. B* **2004**, *108*, 19717–19720.
(35) Snow, E. S.; Perkins, F. K.; Houser, E. J.; Badescu, S. C.; Reinecke, T. L. *Science* **2005**, *307*, 1942–1945.
(36) Tang, J.; Jensen, K.; Li, W.; Waje, M.; Larsen, P.; Ramesh, P.; Itkis, M. E.; Yan, Y.; Haddon, R. *Aus. J. Chem.* **2007**, *60* (7), 528–532.

NL080814U